Inclusive neutron cross sections from Ne-Pb collisions at 790 MeV/nucleon

A. R. Baldwin, R. Madey, W.-M. Zhang, B. D. Anderson, D. Keane, J. Varga,* and J. W. Watson
Kent State University, Kent, Ohio 44242

G. D. Westfall
Michigan State University, East Lansing, Michigan 44823

K. Frankel
Research Medicine and Radiation Biology Division, Lawrence Berkeley Laboratory, Berkeley, California 94720

C. Gale
McGill University, Montreal, Canada H3A-2T8
(Received 9 March 1992)

Inclusive neutron spectra were measured at 0°, 15°, 30°, 50°, 70°, 90°, 120°, and 160° from Ne-Pb collisions at 790 MeV/nucleon. A peak that originates from neutron evaporation from the projectile appears in the spectra at 0°. The shapes and magnitudes of the spectra are compared with those calculated from models of nucleus-nucleus collisions. The Boltzmann-Uehling-Uhlenbeck (BUU), intranuclear cascade (INC), and firestreak models agree generally with the measured double-differential cross sections and particularly at 50° and beyond; however, none of the models can reproduce the peaks at small angles ($\theta \leq 15°$). The quantum molecular dynamics (QMD) model underestimates the spectra of the double-differential cross sections at all angles and energies for this asymmetric system. Also, the predictions of the INC model agrees with the angular distribution of the differential cross sections except that it underestimates the cross section at 0°; the BUU prediction overestimates the differential cross section at 0° and 90°; firestreak overpredicts at 15° and 30° and underpredicts at 70° and 90°; and the QMD model underpredicts the measured angular distribution and the energy spectra at forward angles.

PACS number(s): 25.75.+r

I. INTRODUCTION

The equation of state (EOS) is fundamental for the understanding of the properties of excited nuclear matter and for learning about phase transitions of nuclear matter [1,2]. Although past efforts to extract the EOS were based on a comparison of high-multiplicity-selected data from 4π detectors with theoretical models [3–5], the models have not been tested thoroughly in much simpler measurements of inclusive cross sections. The measurement of double-differential inclusive cross sections is an important supplement to the high-multiplicity-selected data and can help to sort out theoretical descriptions. Agreement between predictions and measurements of inclusive double-differential cross sections over a wide angular region has not been achieved for relativistic collisions of heavy nuclei, and the ability to obtain agreement remains as an important challenge in relativistic heavy-ion physics.

In this paper we report measurements of inclusive double-differential cross sections for neutron emission at 0°, 15°, 30°, 50°, 70°, 90°, 120°, and 160° from 790-MeV/nucleon Ne-Pb collisions. Also, we compare the reported spectra with predictions from four models: (1) firestreak [6,7], (2) intranuclear cascade (INC) [8–11], (3) Boltzmann-Uehling-Uhlenbeck (BUU) transport theory [1,2,4,5,12–15], and (4) quantum molecular dynamics (QMD) [6–18]. We find that none of these approaches can provide overall agreement with the results from this experiment.

II. APPARATUS

The data were taken at the Bevalac accelerator at the Lawrence Berkeley Laboratory. The experimental arrangement is shown in Fig. 1. Eight mean-timed [19] neutron detectors [20] were located at 0°, 15°, 30°, 50°, 70°, 90°, 120°, and 160° with respect to the beam direction. Each detector consisted of an NE-102 plastic scintillator, 10.16 cm thick and 101.6 cm wide; the scintillators at the first five forward angles were 25.4 cm high, and those at the remaining three angles were 50.8 cm high. Neutrons were emitted with a projectile energy of 790 MeV/nucleon at the center of a 3.43-g/cm^2 Pb target oriented at 45° with respect to the beam direction. Charged particles incident on each of the eight neutron detectors were vetoed with either a 6.3-mm- or a 9.5-mm-thick anticoincidence plastic scintillator. The time of flight (TOF) of each detected neutron was determined by measuring the time difference between the detection in one of the neutron detectors and the detection of a Ne ion in a beam telescope, which consisted of two NE-102 (76.2 mm $\times$76.2 mm $\times$0.8 mm thick) scintillation counters positioned about 0.1 and 1.5 m upstream of the

*Present address: 2414 Fortune Avenue, Parma, OH 44314.

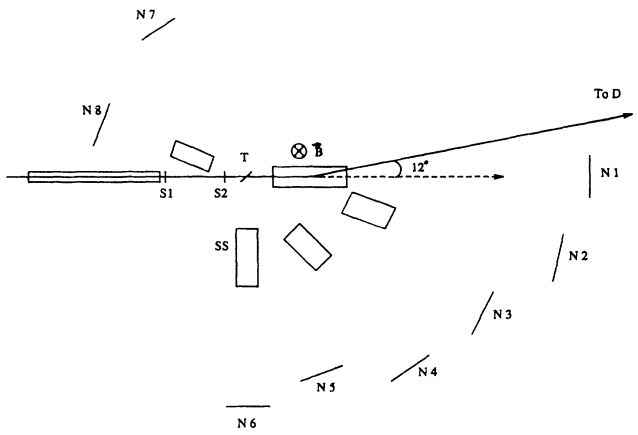

FIG. 1. Experimental arrangement. $N1$ through $N8$ represent eight neutron detectors, $S1$ and $S2$ are the two scintillators of the beam telescope, T is the target, SS denotes shadow shields in one configuration, D is the beam dump, and **B** shows the magnetic field of the C magnet.

target. The flight paths for the eight detectors decreased with increasing polar angle of the detector; as listed in Table I, they vary from 8.06 m at 0°, to 5.55 m at 90°, to 3.57 m at 160°. Neutron energy resolutions at each angle are listed in Table I also for 200-, 800-, and 1500-MeV neutrons. The neutron energy resolution [full width at half maximum (FWHM)] for the detector at 0° varied from 10 MeV at 200 MeV, to 102 MeV at 800 MeV, to 350 MeV at 1500 MeV; at 90°, the neutron energy resolution was 15 MeV at 200 MeV and about 155 MeV at 800 MeV. With a threshold of 12 MeV for protons, the neutron detection efficiency for a 50.8-cm-wide detector, calculated with the Monte Carlo code of Cecil, Anderson, and Madey [21], falls slowly from 9.0% at 150 MeV to about 7.5% at 1000 MeV and beyond. The efficiencies for neutron energies above 500 MeV have not been tested experimentally [20]; however, as pointed out in Ref. [22], the uncertainties in the detection efficiencies do not prevent us from extracting physics results of interest. The detection efficiencies for a 25.4-cm-wide detector were calculated to be not more than 0.5% lower than those for a 50.8-cm-wide detector at all energies.

Auxiliary measurements with steel shadow shields, 121 cm long at 0° and 90° and 102 cm long at the other angles,

TABLE I. Flight paths and energy resolutions (FWHM) for the eight neutron detectors.

Angle	Flight path	Energy resolution (FWHM)		
θ (deg)	x (m)	at 200 MeV	at 800 MeV	at 1500 MeV
0	8.06	10	102	350
15	7.55	11	110	
30	6.55	12	125	
50	6.05	13	135	
70	5.05	15	155	
90	5.55	15	155	
120	4.07	20	200	
160	3.57	23	235	

were used to determine target-correlated backgrounds. The other dimensions were typically 31 cm high by 60 cm wide for the detectors at 0° and 90°; 17 cm high by 54 cm wide for the 25.4-cm-wide detectors at 15°, 30°, 50°, and 70°; and 34.5 cm high by 36 cm wide for the 50.8-cm-wide detectors at 120° and 160°. Each shadow shield was located about halfway between the target and shadowed detector. The 102-cm-long shadow shields attenuated neutrons by a factor $>10^3$ at all energies. There were two configurations for shadow shields: The first configuration shadowed the detectors at 15°, 50°, 90°, and 160°, the second at 0°, 30°, 70°, and 120°.

The intensity of the usable incident beam was about 2×10^5 ions per pulse after a rejection loss of about 60%. Pileup circuitry rejected any beam ion that was accompanied by a second beam ion within a predetermined sampling time of typically ±400 ns. After traversing the beam telescope and target, the beam was deflected by the large-aperture (19.7 cm gap) C magnet through an angle of 12° into a reentrant beam dump.

Events with two neutrons in a detector were indistinguishable from single-neutron events. Based on a subsequent measurement, the ratio of the number of two-neutron events to the number of single-neutron events was negligible within uncertainties.

III. INCLUSIVE SPECTRA

The kinetic energy of each neutron was derived from the measured TOF. Inclusive double-differential cross sections are plotted in Fig. 2 for Ne-Pb collisions at 790 MeV/nucleon as a function of the neutron kinetic energy in the laboratory. The uncertainties are contained within the plotted symbols unless indicated otherwise. The er-

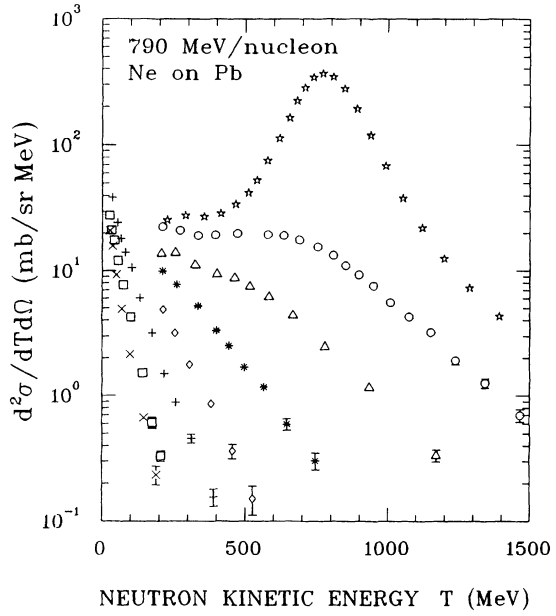

FIG. 2. Inclusive double-differential cross sections for emission of neutrons above 200 MeV at 0° (☆), 15° (○), 30° (△), 50° (*), 70° (◇), 90° (+), 120° (□), and 160° (×) from Ne-Pb collisions at 790 MeV/nucleon vs the neutron kinetic energy in the laboratory.

ror bars reflect the statistical uncertainties. As described in Ref. [23] for the spectra at 0°, the systematic uncertainty from the determination of the proton energy threshold is about 10%. Because of uncertainties from background subtractions, the ability to acquire reliable data at low energies and forward angles was restricted. At high energies the bin widths are smaller than the energy resolution. The spectra at 0°, which were discussed in detail in Ref. [23], are characterized by a high-energy tail and a peak at an energy of 770±15 MeV.

The neutron double-differential cross sections were integrated over neutron kinetic energies above 200 MeV. Plotted in Fig. 3 are the angular distributions of the differential cross sections for emission of neutrons above 200 MeV from Ne-Pb collisions. The total neutron cross sections $\sigma(T>200$ MeV, $0°\leq\theta\leq 90°)$ were obtained by integrating the above differential cross sections over the polar angle region; the results are 19±2 b for Ne-Pb collisions. Exclusion of the polar angle region from 90° to 180° neglects about 1% of the total cross section. The missing cross section was estimated from an exponential extrapolation of the five points (at 15°, 30°, 50°, 70°, and 90°) of the angular distributions in Fig. 3. The average number of neutrons above 200 MeV emitted in a collision is $\sigma(T>200$ MeV, $0°\leq\theta\leq 90°)/\sigma_G=5.9\pm0.6$, where the geometric cross section

$$\sigma_G=\pi(R_P+R_T)^2=\pi r_0^2(20^{1/3}+208^{1/3})^2=3.2 \text{ b} ,$$

for Ne-Pb collisions.

The measurements of inclusive neutron spectra are plotted in Fig. 4 as contours of Lorentz-invariant cross sections for Ne-Pb collisions, respectively, in the space of

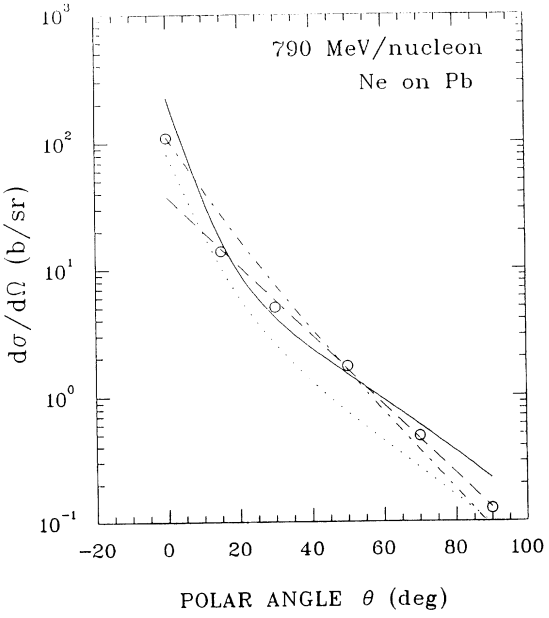

FIG. 3. Inclusive differential cross section for emission of neutrons above 200 MeV from Ne-Pb collisions at 790 MeV/nucleon vs the emission angle. Predictions are shown for BUU (solid line), INC (dashed line), firestreak (dot-dashed line), and QMD (dotted line).

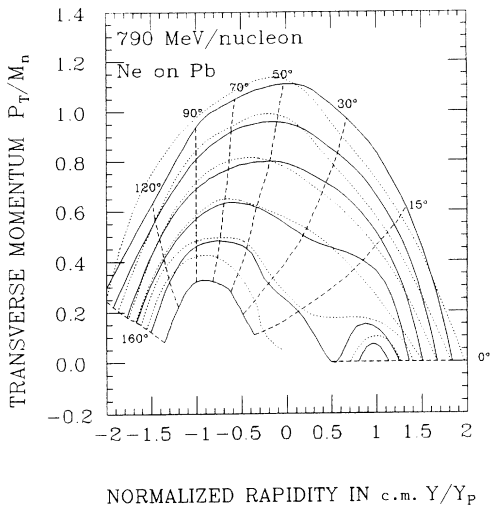

FIG. 4. Contours of Lorentz-invariant cross sections for emission of neutrons from Ne-Pb collisions at 790 MeV/nucleon plotted in the plane of transverse momentum (normalized to the mass of neutron) vs the neutron rapidity in center-of-mass system (normalized to the projectile rapidity). The solid lines represent the data. The dotted lines are BUU calculations. The dashed lines represent the polar angles of the detectors. The values of the Lorentz-invariant cross sections are 0.3 $\mu b\, c^3/\text{MeV}^2\,\text{sr}$ for the outermost contour and 100 $\mu b\, c^3/\text{MeV}^2\,\text{sr}$ for the innermost contour. The values in between are 30, 10, 3, and 1 $\mu b\, c^3/\text{MeV}^2\,\text{sr}$.

transverse momentum P_T (normalized to the neutron mass M_n) versus the neutron rapidity Y (normalized to the projectile rapidity Y_P) in the nucleon-nucleon center-of-mass system. The values of the Lorentz-invariant cross sections are 0.3 $\mu b\, c^3/\text{MeV}^2\,\text{sr}$ for the outermost contour and 100 $\mu b\, c^3/\text{MeV}^2\,\text{sr}$ for the innermost contour. The dashed lines represent the phase space of neutrons detected in the eight detectors from 0° to 160°. The extremities of these lines denote the upper and lower limits of the momenta detected in the experiment. From the figure we see contours centered around a value of the normalized rapidity that is slightly smaller than the projectile rapidity of $Y/Y_p=1$; these contours are produced by spectator neutrons emitted from the projectile. Also, we see contours centered at zero rapidity formed by participant neutrons. Additional contours appear in the vicinity of the target rapidity $Y/Y_p=-1$, which are produced by spectator neutrons emitted from the target. The cross section at the center of the contours around the target rapidity is higher than that at the center of the contours around the projectile rapidity because the mass of the Pb target is larger than that of the Ne projectile. Plotted as dotted lines are predictions of contours from the BUU model. We see that the BUU cross sections agree generally with the data except that the BUU model predicts higher cross sections for the contours centered about the target and projectile rapidities. Because none of the models discussed in the next section include neutron evaporation, predictions from these models do not account for

the evaporation component seen in the spectra at the most forward angles.

IV. COMPARISON WITH MODELS

Here we compare the results from this experiment with four models of nucleus-nucleus collisions: firestreak, intranuclear cascade (INC), Boltzmann-Uehling-Uhlenbeck (BUU), and quantum molecular dynamics (QMD). The firestreak model is a modified version of the fireball model [24]; both of these models are thermodynamic models. The firestreak model includes a forward-backward asymmetry in the center-of-mass system, as observed in experimental data. At angles where thermal processes dominate, firestreak cross sections agree reasonably well with spectra at bombarding energies in the vicinity of a few hundred MeV per nucleon and with spectra from collisions of light-mass systems only at higher bombarding energies up to about 1 GeV per nucleon [7]. The dynamical input is minimal in firestreak. The BUU model [1,2,4,5,12–15] is a microscopic transport theory that is a Monte Carlo solution of the Boltzmann-Uehling-Uhlenbeck equation. It proceeds in terms of a cascade of binary collisions between nucleons and resonances according to the experimental scattering cross sections for free particles, corrected by a Pauli blocking factor. The dependence on the EOS enters via the acceleration of nucleons in the nuclear mean field. The BUU model predicts both collective flow and nucleon cross sections from collision of various systems at different beam energies [4,14,15]; however, because the BUU approach does not account for the formation of composite nuclei, it is possible that the BUU theory will overestimate the measured nucleon cross sections. The intranuclear cascade model does not include compressional energy. The INC calculations presented here estimate the number of free neutrons by subtracting the number of deuteronlike pairs from all neutrons including those in clusters. The QMD model combines the quantum features of the BUU model with a long-range N-body interaction [17–19]. It is of interest to compare the predictions of these models with the measured differential cross sections. The spectra measured in this experiment will test these models for collisions of a light Ne projectile with a heavy Pb target at an energy of 790 Mev/nucleon. A similar comparison was done for collisions of La-La [25], Nb-Nb [26], and Au-Au [26] at an energy of 800 MeV/nucleon.

Predictions of the double-differential cross sections for Ne-Pb collisions are plotted in Figs. 5–8, respectively, for the BUU, INC, QMD, and firestreak models. The statistical uncertainties in the Monte Carlo calculations are comparable with the total uncertainties in the measurements. Because the intranuclear cascade code calculates too many deuterons at low energies as a result of contributions from higher-mass composites, it does not yield reliable predictions of double-differential cross sections at low energies. The BUU code used here is described elsewhere [2,27[. Aichelin *et al.* [25] showed that inclusive spectra are insensitive to the EOS used in nuclear transport models and that models with and without momentum-dependent interactions give similar inclusive

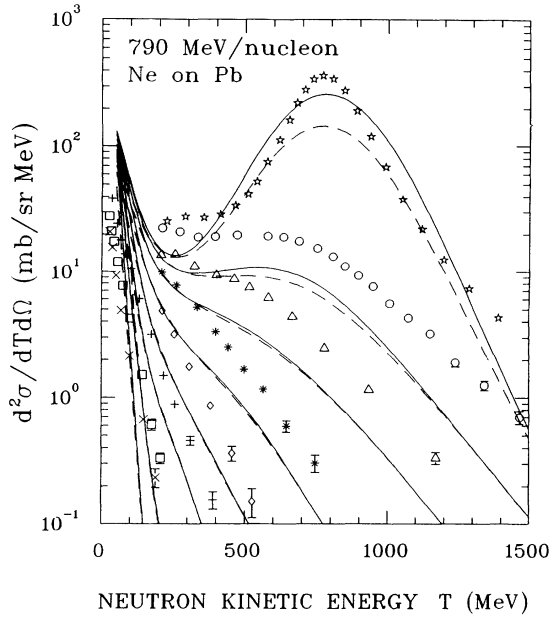

FIG. 5. Predictions from the quantum molecular dynamics (QMD) theory for the inclusive differential cross sections for the emission of neutrons above 200 MeV from Ne-Pb collisions at 790 MeV/nucleon vs the laboratory emission angle. Symbols denote the data: 0° (☆), 15° (○), 30° (△), 50° (*), 70° (◇), 90° (+), 120° (□), and 160° (×). The dashed lines represents the calculation of the free neutrons obtained by subtracting neutrons taken away by composite nuclei. The solid line represents the calculations without accounting for the formation of clusters.

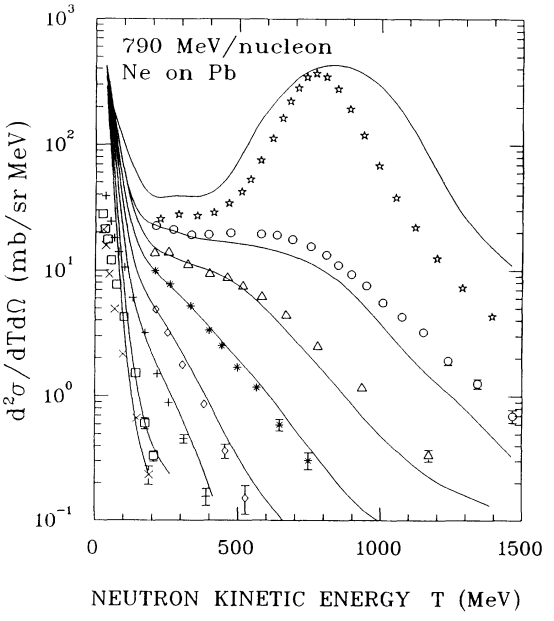

FIG. 6. Predictions from the Boltzmann-Uehling-Uehlenbeck (BUU) theory for the inclusive differential cross sections from the emission of neutrons above 200 MeV from Ne-Pb collisions at 790 MeV/nucleon vs the laboratory emission angle. Symbols denote the data: 0° (☆), 15° (○), 30° (△), 50° (*), 70° (◇), 90° (+), 120° (□), and 160° (×). Solid lines represent theory.

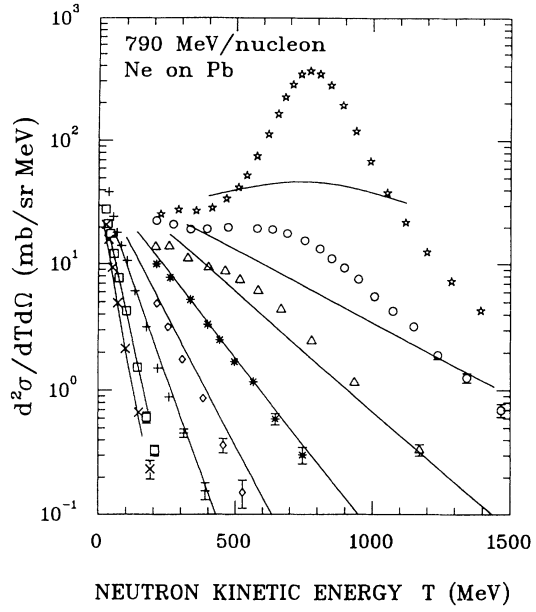

FIG. 7. Predictions from the intranuclear cascade (INC) model for the inclusive differential cross section for the emission of neutrons above 200 MeV from Ne-Pb collisions at 790 MeV/nucleon vs the laboratory emission angle. Symbols denote the data: 0° (☆), 15° (○), 30° (△), 50° (*), 70° (◇), 90° (+), 120° (□), and 160° (×). Solids lines represent theory.

cross sections. The BUU calculations of the spectra presented here used a soft, momentum-dependent interaction as specified by Welke *et al.* [27]. From Fig. 5 we see that the predictions of the QMD calculation underestimate the magnitude of the differential cross sections even when the formation of composites is not taken into account. The QMD calculation shown here takes clustering into account in a crude way: If the spatial separation between the nucleons is less than 1.2 fm, then these nucleons are counted as clusters. Because the version of the QMD code used here carries out the calculation in the nucleon-nucleon center-of-mass system, it is not expected to agree well for this asymmetric Ne-Pb system. The BUU predictions, shown in Fig. 6, provide a reasonable representation of the data except at the smallest angles. We extended the BUU model to include an effective mass correction to the collision integral [28]. This extension makes no significant change to the inclusive spectra except at 0°. A detailed investigation of the effect of this extended BUU model on other observables will be published separately. Aichelin *et al.* [25] showed that the difference between BUU and QMD is small for symmetric La-La collisions at 800 MeV/nucleon. The BUU prediction overestimates the cross section at 0°, whereas the QMD prediction underestimates the cross section at 0°. From Fig. 8 we see that the firestreak model overestimates the differential cross sections in the low-energy region at the most forward angles, and it does not account properly for the peak at 0°. Compared with the data in Fig. 3 are BUU, INC, firestreak, and QMD predictions of the angular distributions of the differential cross sections for emission of neutrons

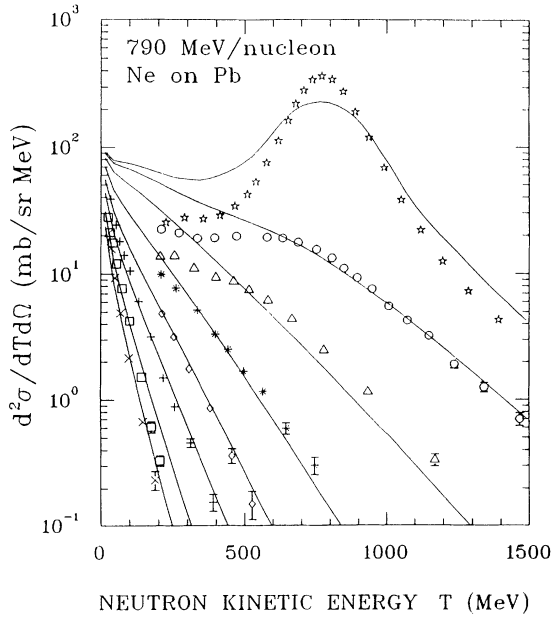

FIG. 8. Predictions from the firestreak model for the inclusive differential cross section for the emission of neutrons above 200 MeV from Ne-Pb collisions at 790 MeV/nucleon vs the laboratory emission angle. Symbols denote the data: 0° (☆), 15° (○), 30° (△), 50° (*), 70° (◇), 90° (+), 120° (□), and 160° (×). Solids lines represent the model.

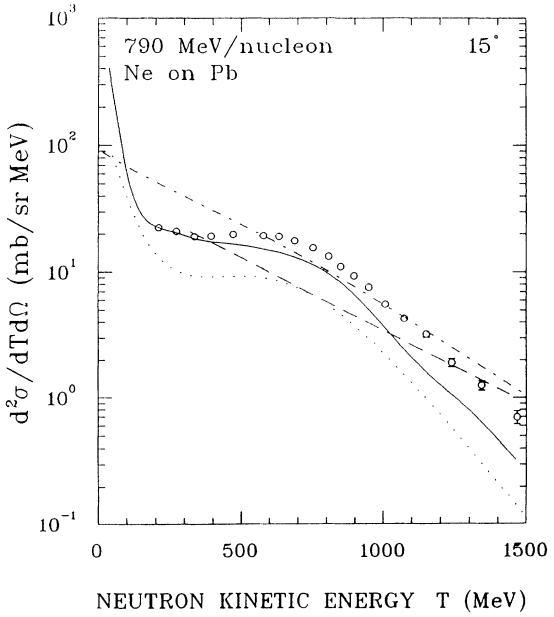

FIG. 9. Predictions for the inclusive double-differential cross sections for neutron emission at 15° from Ne-Pb collisions at 790 MeV/nucleon vs the neutron kinetic energy in the laboratory. Solid, dashed, dot-dashed, and dotted lines represent predictions from BUU, INC, firestreak, and QMD models, respectively. Symbols denote the data.

above 200 MeV. The INC prediction fits best except at 0°, QMD underestimates the data, and BUU overestimates at 0° and 90°; and firestreak overestimates at 15° and 30° and underestimates at 70° and 90°.

For double-differential cross sections at the six polar angles ($\theta > 15°$), we find that the BUU, INC, and firestreak models agree generally with the data, particularly at 50° and beyond, and that the QMD calculation underestimates the differential cross sections at all angles for this asymmetric Ne-Pb system. Although the BUU calculation fits the data best, none of these models can reproduce the peaks at small angles ($\theta \leq 15°$). These forward-angle peaks result from neutron evaporation from the projectile; none of the models describe this process well. In Figs. 9–11 we compare our measurements at three representative angles (viz., 15°, 50°, and 90°) with the predictions from all four models: QMD, BUU, INC, and firestreak. Discrepancies exist at 15° for each model; BUU, INC, and firestreak agree at 50°, whereas QMD underpredicts; INC and firestreak agree with the data at 90° and for neutrons above about 150 MeV; BUU agrees, whereas QMD underpredicts.

The comparisons of the calculated spectra with measured neutron spectra at 0° in Fig. 12 show that a good description of neutron evaporation is needed to account for the measured spectra. Because the BUU calculations include too many free neutrons by not subtracting those that coalesce into clusters, the BUU calculation predicts higher cross sections than those observed.

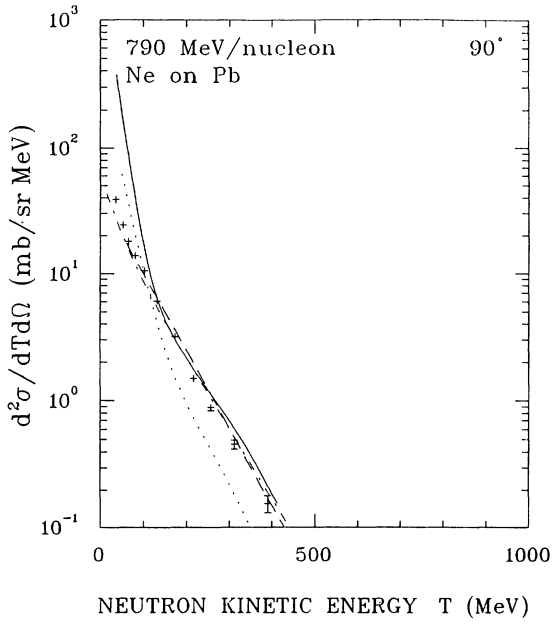

FIG. 11. Predictions for the inclusive double-differential cross sections for neutron emission at 90° from Ne-Pb collisions at 790 MeV/nucleon vs the neutron kinetic energy in the laboratory. Solid, dashed, dot-dashed, and dotted lines represent predictions from BUU, INC, firestreak, and QMD models, respectively. Symbols denote the data.

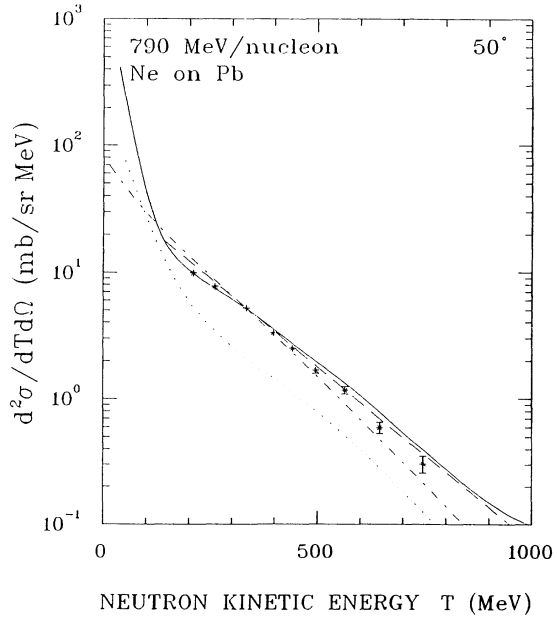

FIG. 10. Predictions for the inclusive double-differential cross sections for neutron emission at 50° from Ne-Pb collisions at 790 MeV/nucleon vs the neutron kinetic energy in the laboratory. Solid, dashed, dot-dashed , and dotted lines represent predictions from BUU, INC, firestreak, and QMD models, respectively. Symbols denote the data.

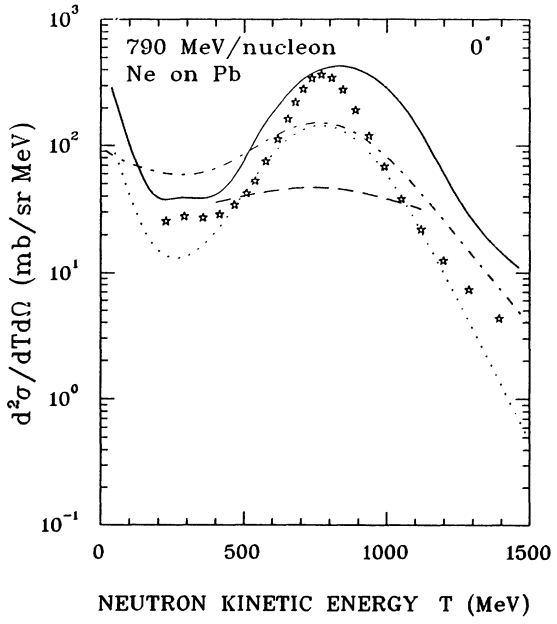

FIG. 12. Predictions for the inclusive double-differential cross sections for neutron emission at 0° from Ne-Pb collisions at 790 MeV/nucleon vs the neutron kinetic energy in the laboratory. Solid, dashed, dot-dashed, and dotted lines represent predictions from the BUU, INC, firestreak, and QMD models, respectively. Symbols denote the data.

V. CONCLUSIONS

We measured inclusive neutron spectra at eight angles 0°, 15°, 30°, 50°, 70°, 90°, 120°, and 160° from Ne-Pb collisions at 790 MeV/nucleon. Neutrons evaporated from an excited projectile appear in the spectra at 0°. Comparisons of the spectra with predictions from the BUU, INC, firestreak, and QMD models show that none of these models account for the evaporative peak at 0°, that QMD underestimates the spectra of the double-differential cross sections at all angles and energies, and that BUU, INC, and firestreak agree generally with the data and particularly at 50° and beyond. Also, predictions of the angular distributions of the differential cross sections do not agree with the measurements over the full angular range.

ACKNOWLEDGMENTS

This work was supported in part by the National Science Foundation under Grant Nos. PHY-88-02392, PHY-85-01054; the Office of Energy Research, Office of Health and Environmental Research Division, of the U.S. Department of Energy under Contract No. DE-AC03-76SF000098; the National Aeronautics and Space Administration, Order No. L14230C; and the Natural Sciences and Engineering Research Council of Canada and the FCAR fund of the Quebec Government.

[1] H. Stöcker and W. Greiner, Phys. Rep. **137**, 278 (1986).
[2] S. Das Gupta and G. Bertsch, Phys. Rep. **160**, 189 (1988).
[3] K. G. R. Doss, H. A. Gustafsson, H. H. Gutbrod, K. H. Kampert, B. Kolb, H. Löhner, B. Ludewigt, A. M. Poskanzer, H. G. Ritter, H. R. Schmidt, and H. Wieman, Phys. Rev. Lett. **57**, 302 (1986).
[4] D. Keane, S. Y. Chu, S. Y. Fung, Y. M. Liu, L. J. Qiao, G. VanDalen, M. Vient, S. Wang, J. J. Molitoris, and H. Stöcker, Phys. Rev. C **37**, 1447 (1988).
[5] P. Danielewicz, H. Ströbele, G. Odyniec, D. Bangert, R. Bock, R. Brockmann, J. W. Harris, H. G. Pugh, W. Rauch, R. E. Renfordt, A. Sandoval, D. Schall, L. S. Schroeder, and R. Stock, Phys. Rev. C **38**, 120 (1988).
[6] W. D. Myers, Nucl. Phys. **A296**, 177 (1978).
[7] J. Gosset, J. I. Kapusta, and G. D. Westfall, Phys. Rev. C **18**, 844 (1978).
[8] J. Cugnon, Phys. Rev. C **22**, 1885 (1980).
[9] Y. Yariv and Z. Fraenkel, Phys. Rev. C **24**, 488 (1981).
[10] J. Cugnon, D. Kinet, and J. Vandermeulen, Nucl. Phys. **A379**, 553 (1982).
[11] J. Cugnon and D. L'Hôte, Phys. Lett. **149B**, 35 (1984).
[12] E. A. Uehling and G. E. Uhlenbeck, Phys. Rev. **43**, 552 (1933).
[13] H. Kruse, B. V. Jacak, and H. Stöcker, Phys. Rev. Lett. **54**, 289 (1985).
[14] H. Kruse, B. V. Jacak, J. J. Molitoris, G. D. Westfall, and H. Stöcker, Phys. Rev. C **31**, 1770 (1985).
[15] G. Bertsch, H. Kruge, and S. Das Gupta, Phys. Rev. C **29**, 672 (1984).
[16] J. J. Molitoris and H. Stöcker, Phys. Rev. C **32**, 346 (1985).
[17] J. Aichelin and H. Stöcker, Phys. Lett. B **176**, 14 (1986).
[18] A. Rosenhauer, G. Peilert, H. Stöcker, and W. Greiner, Phys. Rev. Lett. **58**, 1926 (1987).
[19] A. R. Baldwin and R. Madey, Nucl. Instrum. Methods **171**, 149 (1980).
[20] R. Madey, J. W. Watson, M. Ahmad, B. D. Anderson, A. R. Baldwin, A. L. Casson, W. Casson, R. A. Cecil, A. Fazely, J. M. Knudson, C. Lebo, W. Pairsuwan, P. J. Pella, J. C. Varga, and T. R. Witten, Nucl. Instrum. Methods **214**, 401 (1983).
[21] R. A. Cecil, B. D. Anderson, and R. Madey, Nucl. Instrum. Methods **161**, 439 (1979).
[22] R. Madey, W. M. Zhang, B. D. Anderson, A. R. Baldwin, B. S. Flanders, W. Pairsuwan, J. Varga, J. W. Watson, and G. D. Westfall, Phys. Rev. C **38**, 184 (1988).
[23] R. Madey, J. Varga, A. R. Baldwin, B. D. Anderson, R. A. Cecil, G. Fai, P. C. Tandy, J. W. Watson, and G. D. Westfall, Phys. Rev. Lett. **55**, 1453 (1985).
[24] G. D. Westfall, J. Gosset, P. J. Johansen, A. M. Poskanzer, W. G. Meyer, H. H. Gutbrod, A. Sandoval, and R. Stock, Phys. Rev. Lett. **37**, 1202 (1976).
[25] J. Aichelin, J. Cugnon, Z. Fraenkel, K. Frankel, C. Gale, M. Gyulassy, D. Keane, C. M. Ko, J. Randrup, A. Rosenhauer, H. Stöcker, G. Welke, and J. Q. Wu, Phys. Rev. Lett. **62**, 1461 (1989).
[26] R. Madey, W. M. Zhang, B. D. Anderson, A. R. Baldwin, M. Elaasar, B. S. Flanders, D. Keane, W. Pairsuwan, J. Varga, J. W. Watson, G. D. Westfall, C. Hartnack, H. Stöcker, and K. Frankel, Phys. Rev. C **42**, 1068 (1990).
[27] G. M. Welke, M. Prakash, T. T. S. Kuo, S. Das Gupta, and C. Gale, Phys. Rev. C **38**, 2101 (1988).
[28] V. R. Pandharipande and S. C. Pieper, Phys. Rev. C **45**, 791 (1992).